Pressure-induced successive structural transitions and high-pressure tetragonal phase of $Fe_{1.08}Te$

C. Koz,[1] S. Rößler,[1] A. A. Tsirlin,[1] D. Kasinathan,[1] C. Börrnert,[1] M. Hanfland,[2] H. Rosner,[1] S. Wirth,[1] and U. Schwarz[1,*]

[1]*Max Planck Institute for Chemical Physics of Solids, Nöthnitzer Straße 40, 01187 Dresden, Germany*

[2]*European Synchrotron Radiation Facility, 6 Rue Jules Horowitz, 38043 Grenoble Cedex 9, France*

(Received 21 February 2012; revised manuscript received 22 June 2012; published 5 September 2012)

We report the effects of hydrostatic pressure on the temperature-induced phase transitions in $Fe_{1.08}Te$ in the pressure range 0–3 GPa using synchrotron powder x-ray diffraction. The results reveal a plethora of phase transitions. At ambient pressure, $Fe_{1.08}Te$ undergoes simultaneous first-order structural symmetry-breaking and magnetic phase transitions, namely, from the paramagnetic tetragonal ($P4/nmm$) to the antiferromagnetic monoclinic ($P2_1/m$) phase. We show that, at a pressure of 1.33 GPa, the low-temperature structure adopts an orthorhombic symmetry. More importantly, for pressures of 2.29 GPa and higher, a symmetry-conserving tetragonal-tetragonal phase transition has been identified from a change in the c/a ratio of the lattice parameters. The succession of different pressure and temperature-induced structural and magnetic phases indicates the presence of strong magnetoelastic coupling effects in this material.

DOI: 10.1103/PhysRevB.86.094505 PACS number(s): 74.70.Xa, 74.62.Fj, 61.50.Ks

I. INTRODUCTION

The recent discovery of superconductivity in a Fe-based layered system by Kamihara *et al.*[1] opened up avenues for research in the field of high-transition-temperature superconductivity. The parent compounds of the Fe superconductors display ubiquitous magnetic and structural phase transitions. In this context, the situation is similar to the cuprates for which the exact nature of the intricate interplay between structure, magnetism, and superconductivity still remains elusive after more than two decades of intense research. Since the electronic and phononic excitations are extremely sensitive to the interatomic distances, high pressure can efficiently be used as a clean tuning parameter to systematically influence and, hence, gain insight into these complex ordering phenomena. The physical properties of Fe pnictides and chalcogenides display strong pressure dependencies.[2] In the case of the 1111 and 122 families of compounds, pressure suppresses the magnetic transition temperature T_N (Refs. 3 and 4) and concomitantly enhances the superconducting transition temperature T_c,[5] which suggests an intimate relationship between the two order parameters. Under pressure, some 1111 compounds (e.g., CaFeAsF) undergo a transition from the orthorhombic to lower-symmetry monoclinic phase,[6] in contrast to the transition from orthorhombic to higher-symmetry tetragonal phase found in 122-type compounds.[7] In undoped $BaFe_2As_2$ and $SrFe_2As_2$, pressure induces superconductivity with T_c as high as 38 K.[8–11] Pressure-induced superconductivity in the case of $CaFe_2As_2$ is controversial.[12,13] However, all 122 systems exhibit a tetragonal collapsed phase that seems to exclude superconductivity.[14–16]

Among the different families of Fe superconductors, the tetragonal $Fe_{1+y}Se$ with $T_c = 8$ K can be considered as a reference material owing to its archetypical binary atomic pattern.[17] The structure belongs to the tetragonal $P4/nmm$ space group and consists of edge-sharing $FeSe_4$ tetrahedra, which form layers orthogonal to the c axis. The subtle interplay of structural and physical properties in $Fe_{1+y}Se$ is obvious from the fact that superconducting $Fe_{1.01}Se$ undergoes a structural transition from the tetragonal to the orthorhombic phase at 90 K while nonsuperconducting $Fe_{1.03}Se$ does not.[18] Moreover, $Fe_{1.01}Se$ displays the largest pressure coefficient in the family of Fe-based superconductors, with T_c raising up to 37 K under a pressure of 7–9 GPa.[19–21] Eventually, T_c drops with further increase in pressure, and the crystal structure becomes hexagonal above a pressure of 25 GPa.[20] In addition, T_c of $Fe_{1+y}Se$ can also be enhanced by Te substitution up to a maximum of $T_c = 15$ K for $Fe_{1+y}Se_{0.5}Te_{0.5}$.[22–24] The bulk superconductivity disappears for higher Te substitution and no superconductivity has been found so far in bulk samples of the end-member $Fe_{1+y}Te$. Instead, $Fe_{1+y}Te$ displays a unique interplay of magnetic and structural transitions in dependence on the amount of excess Fe, which is presumably accommodated in interstitial sites.[25–30] The single, first-order magnetic and structural transition to the monoclinic $P2_1/m$ space group observed at $T \approx 69$ K in $Fe_{1.06}Te$ systematically decreases in temperature down to 57 K with an increase in y from 0.06 to 0.11. For $y \geqslant 0.12$, two distinct magnetic and structural transitions occur: the magnetic transition takes place at a *higher* temperature than the structural one.[29] Further, for $y \geqslant 0.12$, the low-temperature structure adopts orthorhombic symmetry, $Pmmn$.[25,28,29] This space group $Pmmn$ is a maximal nonisomorphic subgroup of $P4/nmm$ with index 2. In turn, the space group $P2_1/m$ of the monoclinic arrangement is a maximal nonisomorphic subgroup of this orthorhombic variety with index 2.

So far, high-pressure structural investigations on $Fe_{1+y}Te$ are limited to ambient temperatures.[31,32] A pressure-induced tetragonal lattice collapse has been reported for $Fe_{1.05}Te$ and $Fe_{1.087}Te$ at 300 K at a pressure of about 4 GPa.[31,32] This collapsed tetragonal phase was found to be stable up to a pressure of 10 GPa. However, the magnetic and resistive anomalies observed in a high-pressure study of $FeTe_{0.92}$ (corresponding to $Fe_{1.086}Te$, see Ref. 33) by Okada *et al.*[34] suggested the presence of two pressure-induced phases at low temperatures. This succession of phase transitions resembles the result[29] obtained at ambient pressure but for higher Fe content, $y = 0.13$. In order to clearly cross-correlate the influences on the structure exerted by either pressure or Fe excess, we have chosen to investigate a sample with $y = 0.08$. For this composition, which is close to the one used in Ref. 34, we determine the structure with increasing pressure $p \leqslant 3$ GPa

and compare the observed structural transformations to the influence of chemical composition.

II. EXPERIMENTAL

Polycrystalline samples were synthesized by solid-state reaction of Fe (Alfa Aesar, 99.995%) and Te pieces (Chempur, 99.9999%) in glassy carbon crucibles covered with lids. Mixtures of the target composition were placed in the sample containers and sealed in quartz ampules under vacuum (10^{-5} mbar). After heating to 973 K with a rate of 100 K/h, the samples were kept at this temperature for 24 h before increasing the temperature further up to 1173 K. The dwelling at 1173 K for 12 h was followed by fast cooling to 973 K and annealing for 5 h. Finally, samples were cooled to room temperature at a rate of 100 K/h. Handling of starting materials and products was performed in argon-filled glove boxes. The synthesized samples were characterized by x-ray powder diffraction using Co Kα_1 radiation ($\lambda = 1.788965$ Å) and wavelength dispersive x-ray (WDX) analysis. The results clearly show that the samples selected for the present investigation are single phase with tetragonal symmetry, $P4/nmm$. According to chemical analysis, the samples contain less oxygen and carbon than the detection limit of 0.05 and 0.06 mass percent, respectively. As the physical properties

TABLE I. Parameters of crystal structures and refinements, atomic positions, and atomic displacement parameters U_{iso} (in 10^{-2} Å^2) in the tetragonal phase at 285 K and in the monoclinic phase at 20 K.

	285 K	20 K
Space group	$P4/nmm$	$P2_1/m$
a (Å)	3.82326(4)	3.83367(8)
b (Å)	$= a$	3.78932(7)
c (Å)	6.2824(1)	6.2594(1)
β (deg)	90	90.661(1)
R_I/R_P	0.022/0.067	0.015/0.095
Number of reflections	121	361
Refined parameters for profile/crystal structure	20/6	29/11
Atomic parameters		
Fe1	$2a$ ($\frac{3}{4},\frac{1}{4}$,0)	$2e(x,\frac{1}{4},z)$
	$U_{iso} = 0.93(2)$	$x = 0.7379(4)$
		$z = 0.0014(3)$
		$U_{iso} = 0.23(2)$
Fe2[a]	$2c$ ($\frac{1}{4},\frac{1}{4},z$)	$2e$ ($x,\frac{1}{4},z$)
	$z = 0.720(1)$	$x = 0.238(4)$
	$U_{iso} = 0.9(1)$	$z = 0.719(2)$
		$U_{iso} = 0.4(2)$
Te	$2c$ ($\frac{1}{4},\frac{1}{4},z$)	$2e$ ($x,\frac{1}{4},z$)
	$z = 0.2807(6)$	$x = 0.2431(2)$
	$U_{iso} = 1.08(1)$	$z = 0.2810(1)$
		$U_{iso} = 0.21(1)$

[a]Atomic displacement parameters, U_{iso}, and occupancies are intrinsically correlated and, therefore, cannot be refined independently. Rietveld refinements performed with the nominal composition $Fe_{1.08}Te$ yielded unreasonably small or even negative values for U_{iso}. Realistic values of U_{iso} could be obtained with SOF(Fe2) = 0.09 corresponding to $Fe_{1.09}Te$.

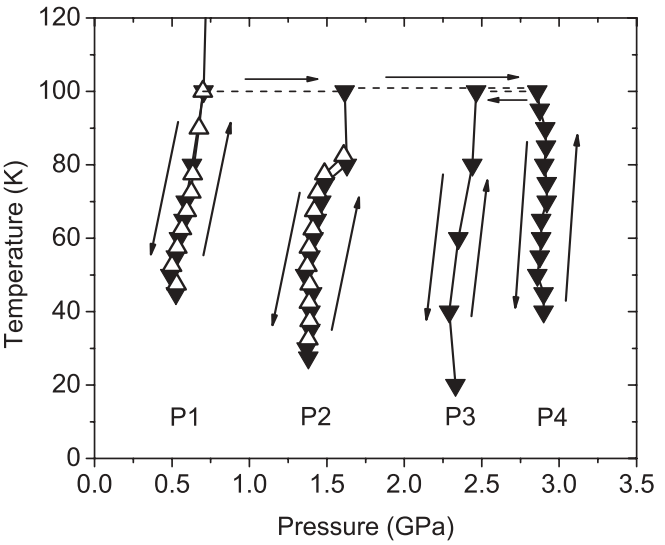

FIG. 1. Experimental protocol: variation of pressure (P) within the four series (referred to as P1–P4) upon changing temperature (T) during the diffraction experiments. ▼ represent P, points at which diffraction data were collected upon cooling; △ mark those measured upon increasing temperature. The temperature-pressure path followed in our experiment is indicated by arrows.

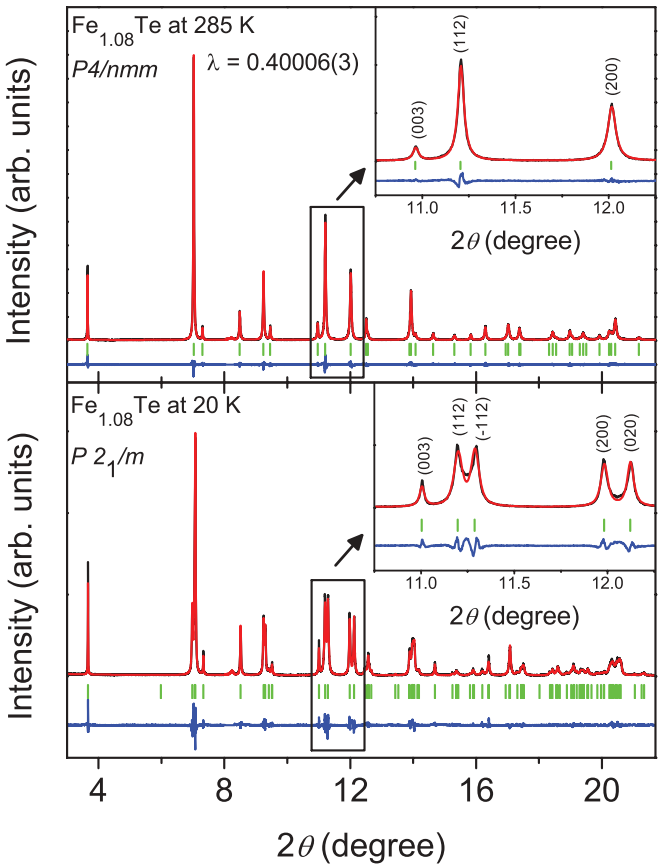

FIG. 2. (Color online) Refined synchrotron powder x-ray-diffraction patterns of $Fe_{1.08}Te$ at temperatures above (285 K) and below (20 K) the phase transition ($T_s \sim 65$ K) at ambient pressure.

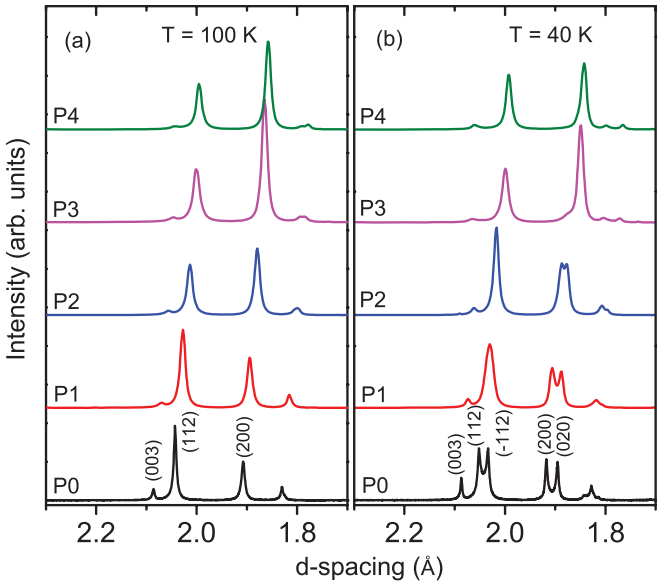

FIG. 3. (Color online) Representative high-pressure XRD patterns of $Fe_{1.08}Te$ at pressures between ambient (P0) and 2.9 GPa (P4), (a) at 100 K and (b) at 40 K.

of $Fe_{1+y}Te$ depend sensitively on the actual Fe content y, emphasis was put on its determination. The amount of Fe as obtained by an inductively coupled plasma method is systematically 1–2% higher than the nominal composition. On the other hand, WDX analysis reveals an amount of iron that is typically 3–4% lower. However, within the estimated experimental error the results are consistent with the nominal composition. More importantly and in satisfactory agreement, Rietveld refinements of high-resolution synchrotron powder x-ray-diffraction (XRD) data indicate a composition $Fe_{1.09}Te$ for the nominal composition $Fe_{1.08}Te$ (see Table I). Similar subtle variations of the determined amount of Fe result also from alternative analysis methods as was reported independently.[30]

Our earlier study[29] on $Fe_{1.08}Te$ revealed a sharp first-order transition at $T_s \sim 65$ K in the heat capacity $C_p(T)$ accompanied by an anomaly in the temperature dependence of the electrical resistivity $\rho(T)$ and the magnetic susceptibility $\chi(T)$, corresponding to a simultaneous magnetic and structural transition. In order to investigate this transition in detail, powder XRD experiments were performed in an angle-dispersive mode at the beam lines ID31 and ID09A of the ESRF (ID31: $\lambda = 0.40006(3)$ Å or 0.39993(3) Å, ID09A: $\lambda = 0.415165$ Å). Temperatures down to $T = 20$ K, both at ambient and elevated pressure, were realized utilizing special He-flow cryostats adapted to the requirements of the diffraction setup environment. The powdered samples were taken in a thin-wall borosilicate glass capillary for ambient pressure measurements (ID31). High pressures were generated by means of the diamond anvil cell technique. The samples were placed in spark-eroded holes of preindented metal gaskets, together with small ruby spheres for pressure determination and liquid helium as a force-transmitting medium (ID09A). The protocol used for the pressure experiment is presented in Fig. 1. Lattice parameters were determined using the program

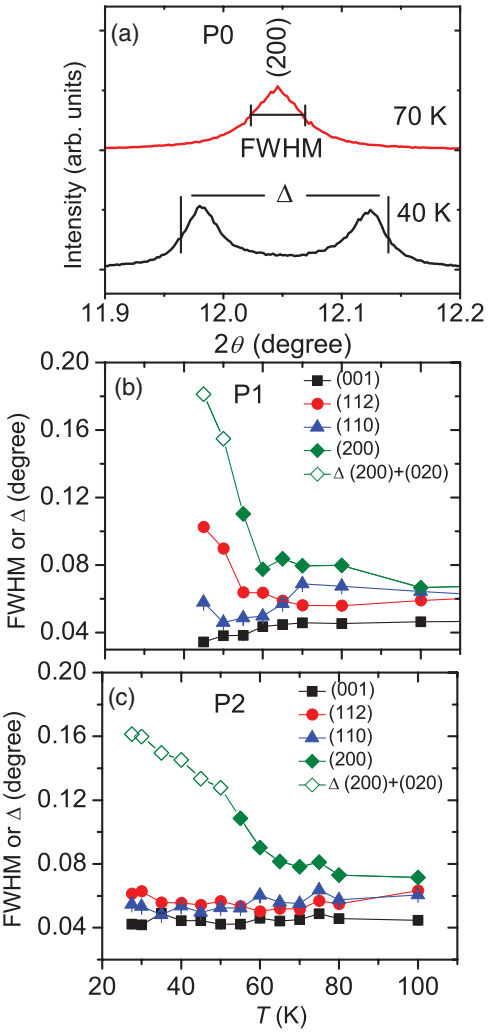

FIG. 4. (Color online) Temperature dependence of powder x-ray-diffraction peaks of $Fe_{1.08}Te$. (a) For characterizing the symmetry-breaking transition, the full width at half maximum (FWHM) or (for visible splitting) the sum Δ of the separation of peak maxima plus FWHM, respectively, of selected reflections. (b) The broadened pattern involving, e.g., the reflections (112) and (200) evidencing monoclinic distortion at low temperatures in the pressure regime P1, whereas (c) constant values for all peaks except (200) indicate an orthorombic low-temperature phase at P2. The error bars are smaller than the symbol sizes.

package WinCSD,[35] and refinements of the crystal structures were performed on the basis of full diffraction profiles with JANA.[36] In these least-squares procedures, the considerable effects of preferred orientation caused by the anisotropy of the crystal structure are accounted for by the March-Dollase formalism.[37,38]

III. RESULTS AND DISCUSSION

A full-profile refinement of powder XRD data measured at ambient pressure confirmed a temperature-induced transformation from tetragonal $Fe_{1.08}Te$ (space group $P4/nmm$ at 285 K) into the monoclinic phase ($P2_1/m$ at 20 K) at low temperature (Fig. 2). Consistent with earlier results,[25] the

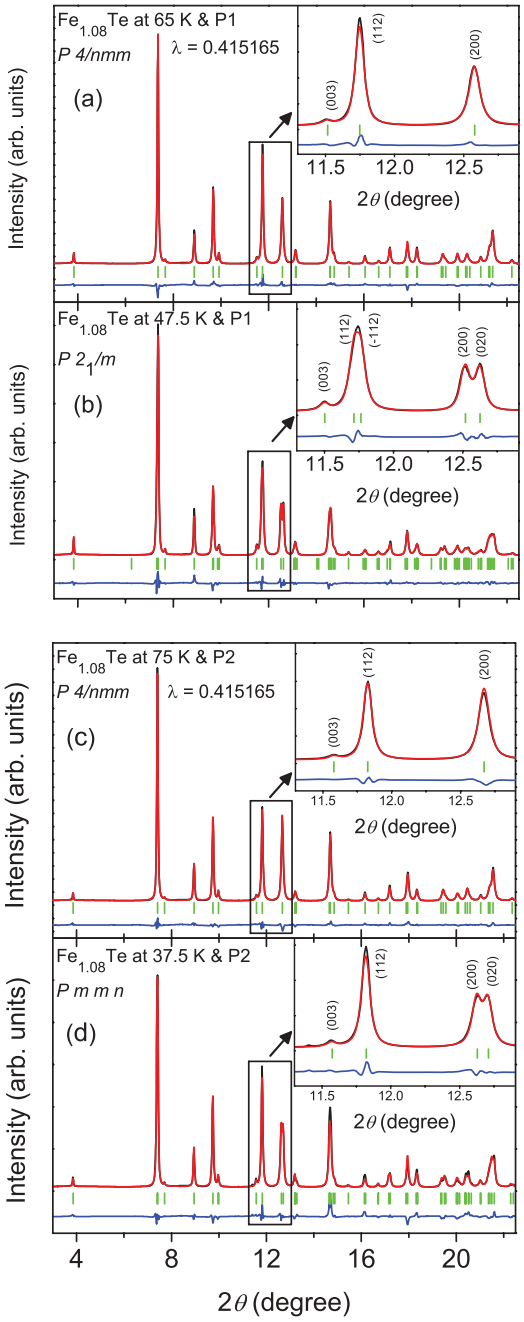

FIG. 5. (Color online) Refined synchrotron powder x-ray-diffraction patterns of $Fe_{1.08}Te$ for the series P1 at temperatures (a) above (65 K) and (b) below (47.5 K) the tetragonal-to-monoclinic transition. (c) and (d) At P2, an observed transition from tetragonal to orthorhombic phase.

phase transition is obvious from a clear splitting of Bragg peaks like (112) and (200). Refined structural parameters at 285 and 20 K are presented in Table I.

Powder XRD patterns of $Fe_{1.08}Te$ in the region of the (112) and (200) Bragg peaks recorded for four different pressure values up to 3 GPa are displayed in Fig. 3. At a temperature of 100 K [Fig. 3(a)], the diagrams evidence the stability of the tetragonal phase within the complete pressure range.

TABLE II. Parameters of crystal structures and refinements, atomic positions, and atomic displacement parameters U_{iso} (in 10^{-2} Å^2) at temperatures above and below the phase transition in the pressure ranges P1 and P2.

	65 K, 0.58 GPa (P1)	47.5 K, 0.53 GPa (P1)
Space group	$P4/nmm$	$P2_1/m$
a (Å)	3.7899(1)	3.8076(1)
b (Å)	$= a$	3.7758(1)
c (Å)	6.2081(2)	6.2147(3)
β (deg)	90	90.354(3)
R_I/R_P	0.025/0.038	0.017/0.040
Number of reflections	39	104
Refined parameters for profile/crystal structure	22/6	27/9
Atomic parameters		
Fe1	$2a$ $(\frac{3}{4},\frac{1}{4},0)$	$2e(x,\frac{1}{4},z)$
	$U_{iso} = 0.29(5)$	$x = 0.735(1)$
		$z = 0.0022(9)$
		$U_{iso} = 0.31(6)$
Fe2[a]	$2c$ $(\frac{1}{4},\frac{1}{4},z)$	$2e$ $(x,\frac{1}{4},z)$
	$z = 0.711(4)$	$x = 0.24(1)$
	$U_{iso} = 1.5(5)$	$z = 0.729(4)$
		$U_{iso} = 0.30$ (fixed)
Te	$2c$ $(\frac{1}{4},\frac{1}{4},z)$	$2e$ $(x,\frac{1}{4},z)$
	$z = 0.2841(1)$	$x = 0.2480(6)$
	$U_{iso} = 0.19(3)$	$z = 0.2827$ (2)
		$U_{iso} = 0.09(3)$
	75 K, 1.49 GPa (P2)	37.5 K, 1.39 GPa (P2)
Space group	$P4/nmm$	$Pmmn$
a (Å)	3.7620(2)	3.7746(4)
b (Å)	$= a$	3.7506(4)
c (Å)	6.1735(4)	6.1757(7)
β (deg)	90	90
R_I/R_P	0.027/0.036	0.051/0.059
Number of reflections	39	62
Refined parameters for profile/crystal structure	25/6	24/6
Atomic parameters		
Fe1	$2a$ $(\frac{3}{4},\frac{1}{4},0)$	$2b(\frac{3}{4},\frac{1}{4},z)$
	$U_{iso} = 0.10(5)$	$z = 0.0141(1)$
		$U_{iso} = 0.28(7)$
Fe2[a]	$2c$ $(\frac{1}{4},\frac{1}{4},z)$	$2a$ $(\frac{1}{4},\frac{1}{4},z)$
	$z = 0.710(4)$	$z = 0.699(6)$
	$U_{iso} = 0.8(4)$	$U_{iso} = 1.00$ (fixed)
Te	$2c$ $(\frac{1}{4},\frac{1}{4},z)$	$2a$ $(\frac{1}{4},\frac{1}{4},z)$
	$z = 0.2867(1)$	$z = 0.2862(2)$
	$U_{iso} = 0.42(3)$	$U_{iso} = 0.28(4)$

The visible peaks shift upon increasing pressure, indicating a continuous compression. At around 2.9 GPa, the lattice parameters a and c are 2.6 and 2.0% smaller than those at ambient pressure, respectively. This decrease in lattice parameters with pressure at 100 K is slightly smaller than the recently reported results for 300 K.[31,32]

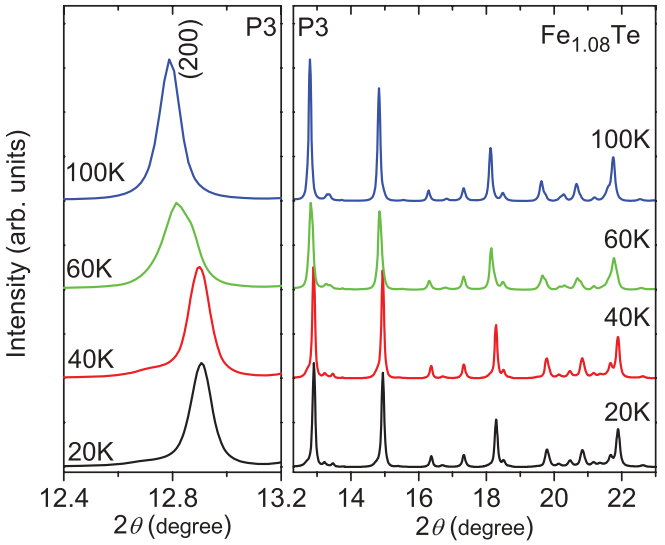

FIG. 6. (Color online) Powder x-ray-diffraction patterns of $Fe_{1.08}Te$ in the pressure regime P3 at low temperatures. The left part displays the region of the (200) reflection and the right part displays an overview of the broader angular range. The pattern at 100 K shows the tetragonal high-temperature phase. The shoulder of the (200) reflection visible at higher angles in the diffraction data taken at 60 K is assigned to the admixture of a second modification. The diagrams recorded at 40 and 20 K exhibit the tetragonal low-temperature phase. The pronounced shift of, e.g., the (200) line evidences a significant change of the unit cell parameters associated with the symmetry-conserving transformation.

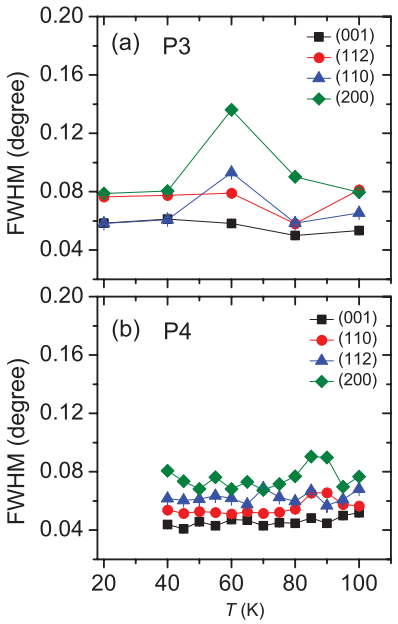

FIG. 7. (Color online) Full width at half maximum of selected reflections in the powder x-ray-diffraction diagrams of $Fe_{1.08}Te$ as a function of temperature at (a) pressure P3 = 2.29–2.47 GPa and (b) pressure P4 = 2.86–2.92 GPa. The increased values around 60 K in the pressure range P3 or 90 K for P4 are attributed to transitions from the tetragonal high-temperature into the tetragonal low-temperature phase involving two-phase regions. The error bars are smaller than the symbol sizes.

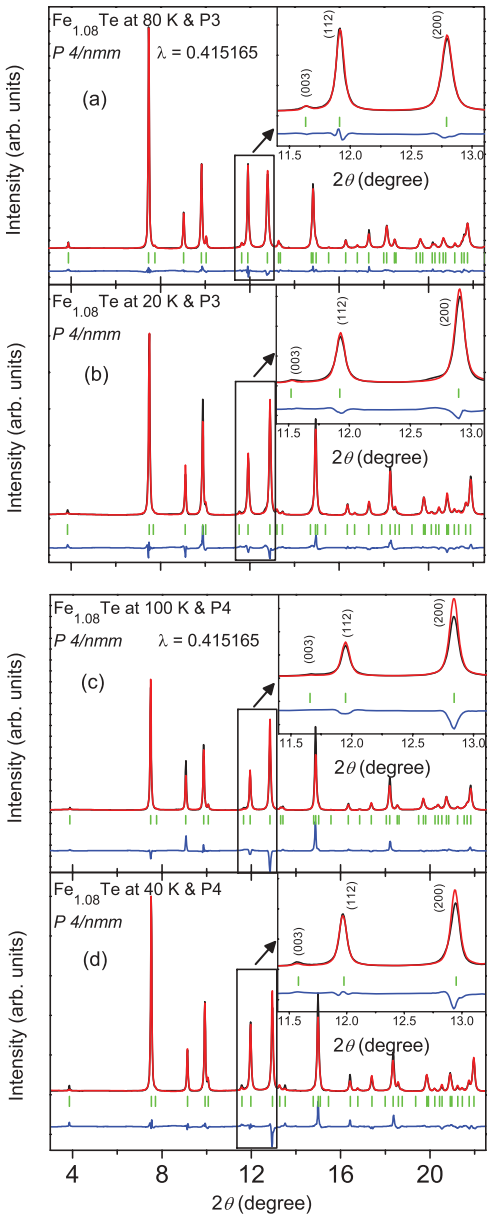

FIG. 8. (Color online) Refined synchrotron powder x-ray-diffraction patterns of $Fe_{1.08}Te$ for (a) and (b) series P3 and (c) and (d) series P4. Shown are results at characteristic temperatures above [(a) 80 K, (c) 100 K] and below [(b) 20 K, (d) 40 K] the symmetry-conserving tetragonal-tetragonal phase transition.

Upon cooling at only slightly elevated pressures (series P1, pressure values from 0.31–0.75 GPa dependent on temperature, see Fig. 1), additional diffraction lines indicate the onset of a structural change at 55 K. At this temperature, two phases are identified in the XRD patterns of $Fe_{1.08}Te$. At lower temperatures, line broadening of the (112) reflection and a successive splitting of the (200) peak are observed [Fig. 3(b)]. In order to characterize the phase transition, the full width at half maximum (FWHM), as well as the sum Δ of separation of peak maxima plus FWHM, are depicted in Fig. 4. With decreasing temperature, the refined FWHM value of the (112) peak approximately doubles: from 0.0512(2)°

TABLE III. Parameters of crystal structures and refinements, atomic positions, and atomic displacement parameters U_{iso} (in 10^{-2} Å^2) for the pressure ranges P3 and P4.

	80 K, 2.44 GPa (P3)	20 K, 2.33 GPa (P3)
Space group	$P4/nmm$	$P4/nmm$
a (Å)	3.7265(1)	3.6946(1)
b (Å)	$= a$	$= a$
c (Å)	6.1428(3)	6.2010(5)
β (deg)	90	90
R_I/R_P	0.024/0.036	0.059/0.073
Number of reflections	35	36
Refined parameters for profile/crystal structure	23/5	26/5
Atomic parameters		
Fe1	$2a$ ($\frac{3}{4}$,$\frac{1}{4}$,0)	$2a$($\frac{3}{4}$,$\frac{1}{4}$,0)
	$U_{iso} = 0.53(5)$	$U_{iso} = 0.43(7)$
Fe2	$2c$ ($\frac{1}{4}$,$\frac{1}{4}$,z)	$2c$ ($\frac{1}{4}$,$\frac{1}{4}$,z)
	$z = 0.680(4)$	$z = 0.662(6)$
	$U_{iso} = 0.4(4)$	$U_{iso} = 0.4$ (fixed)
Te	$2c$ ($\frac{1}{4}$,$\frac{1}{4}$,z)	$2c$ ($\frac{1}{4}$,$\frac{1}{4}$,z)
	$z = 0.2911(2)$	$z = 0.2955(3)$
	$U_{iso} = 0.36(3)$	$U_{iso} = 0.11(5)$
	100 K, 2.86 GPa (P4)	40 K, 2.90 GPa (P4)
Space group	$P4/nmm$	$P4/nmm$
a (Å)	3.7131(6)	3.6835(1)
b (Å)	$= a$	$= a$
c (Å)	6.1316(12)	6.1769(5)
β (deg)	90	90
R_I/R_P	0.076/0.089	0.077/0.074
Number of reflections	42	42
Refined parameters for profile/crystal structure	23/3	22/5
Atomic parameters		
Fe1	$2a$ ($\frac{3}{4}$,$\frac{1}{4}$,0)	$2a$ ($\frac{3}{4}$,$\frac{1}{4}$,0)
	$U_{iso} = 0.3$ (fixed)	$U_{iso} = 0.95(7)$
Fe2	$2c$ ($\frac{1}{4}$,$\frac{1}{4}$,z)	$2c$ ($\frac{1}{4}$,$\frac{1}{4}$,z)
	$z = 0.68(1)$	$z = 0.661(6)$
	$U_{iso} = 0.3$ (fixed)	$U_{iso} = 0.3$ (fixed)
Te	$2c$ ($\frac{1}{4}$,$\frac{1}{4}$,z)	$2c$ ($\frac{1}{4}$,$\frac{1}{4}$,z)
	$z = 0.2922(4)$	$z = 0.2948(3)$
	$U_{iso} = 0.3$ (fixed)	$U_{iso} = 0.21(4)$

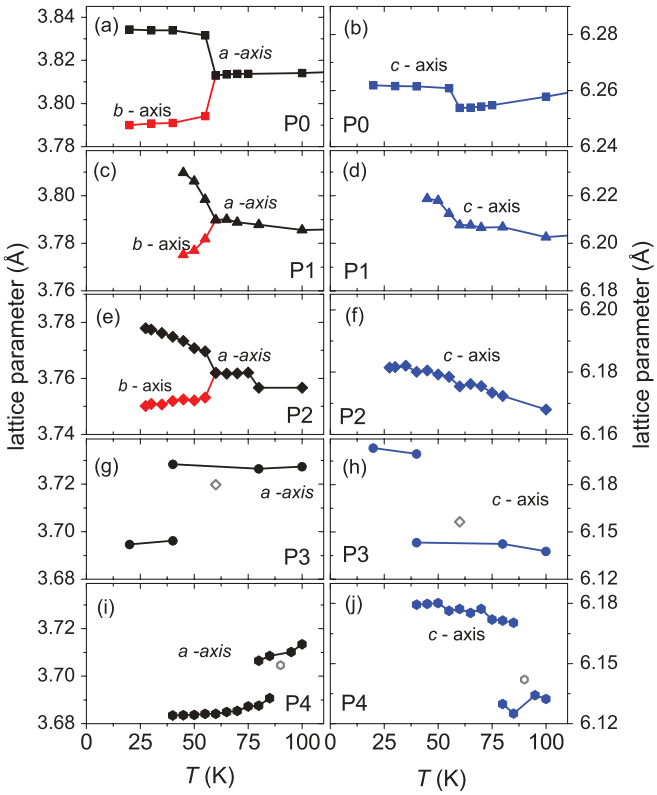

FIG. 9. (Color online) Temperature dependence of lattice parameters a–c at various pressures up to 3 GPa. (a)–(d) A transition from tetragonal to monoclinic symmetry seen at ambient pressure P0 and for pressure P1. (e) and (f) For P2, an orthorhombic phase found at $T \lesssim 60$ K. Another transition appears to occur at $T \approx 75$ K. (g)–(j) A pronounced lattice change within the tetragonal symmetry observed for P3 and P4. Open symbols show average values for mixtures of the high- and low-temperature phases in P3 and P4. Note a slight temperature-induced decrease of pressure in the experimental setup upon cooling (see Fig. 1 and Appendix).

at 295 K to 0.1025(1)° at 40 K [Fig. 4(b)]. Indexing of the reflections at low temperature requires monoclinic symmetry compatible with the ambient pressure low-temperature phase, $P2_1/m$. Crystal-structure refinements of both high- and low-temperature modification are shown in Figs. 5(a) and 5(b), and the refined parameter values are listed in Table II.

At slightly higher pressure (series P2, 1.38–1.65 GPa), the broadening of the (112) peak at low temperatures is completely suppressed [FWHM at 100 K: 0.0613(1)°; 27.5 K: 0.0631(2)°] while the splitting of the (200) and (020) Bragg peaks remains clearly visible [Fig. 4(c)]. Owing to the modified XRD pattern, the diagrams measured at temperatures of 55 K and below require an orthorhombic lattice for indexing. Systematic extinctions are compatible with space group $Pmmn$. Consistently, a first Le Bail refinement yields similarly low values of the residuals as the fit of a monoclinic model. However, the orthorhombic pattern involves a smaller number of free parameters, and thus the higher-symmetry $Pmmn$ model is selected for the crystal-structure refinements using full diffraction profiles. The results for the low- and high-temperature modifications are visualized in Figs. 5(c) and 5(d), and refined parameter values are included in Table II. Upon further increase in pressure (series P3, 2.29–2.47 GPa, and P4, 2.86–2.92 GPa), cooling of the samples induces broadening or the formation of shoulders for some peaks (Fig. 6). For instance, in the series P3, the determined FWHM of peak (200) corresponds to 0.0797(2)° at 100 K, then increases to 0.1362(2)° at 60 K, and finally decreases to 0.0784(1)° at 20 K [Fig. 7(a)]. The patterns of the observed changes in the series P3 and P4 clearly indicate a temperature-induced phase transition involving a two-phase region in which both modifications coexist. Phase coexistence is evidenced between

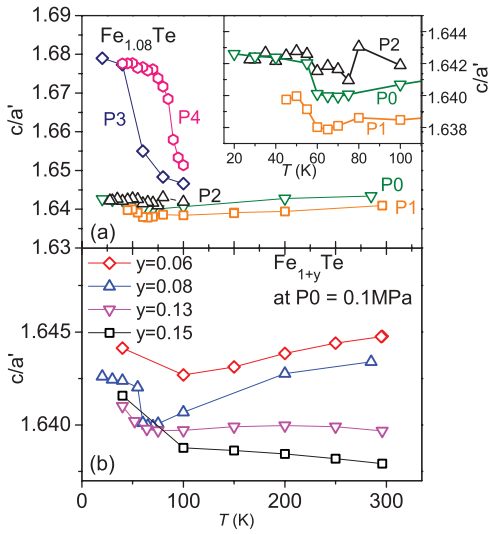

FIG. 10. (Color online) Temperature dependence of c/a' where $a' = a$ for tetragonal symmetry, or equivalently $a' = \frac{1}{2}(a+b)$ for orthorhombic and monoclinic symmetries at (a) various pressures on $Fe_{1.08}Te$ (i.e., $y = 0.08$) (Inset: data sets P0–P2 at low temperatures magnified for clarity) and (b) various amounts y of interstitial Fe at ambient pressure.

60 and 40 K at P3 and between 90 and 80 K at P4 [Fig. 7(b)]. Coexisting phases in a very large pressure range have also been reported in the case of pnictide compounds at low temperatures.[6,7]

A detailed analysis of the line positions revealed that upon cooling Bragg peaks like (200) exhibit strong shifts towards higher 2θ angles whereas reflections like $(00l)$ are reallocated at lower values of 2θ [see, e.g., the (003) peak in the insets to Fig. 8]. This finding implies that the phase transition into the

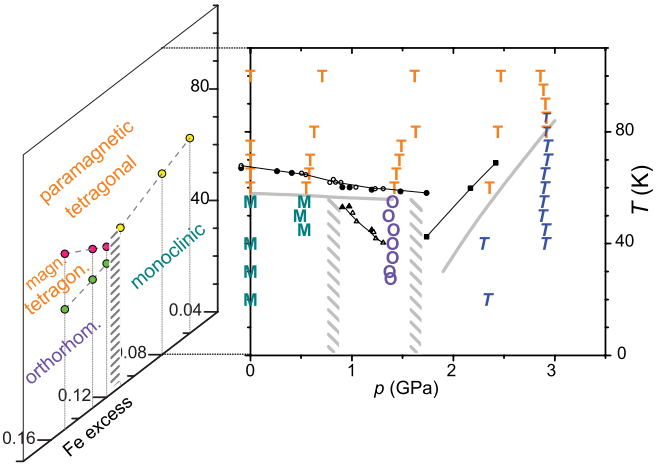

FIG. 11. (Color online) Temperature-pressure-composition phase diagram for the $Fe_{1+y}Te$ system. Symbols T, M, and O mark temperatures and pressures of our XRD measurements revealing tetragonal, orthorhombic, and monoclinic phases, respectively. The black data points indicate anomalies in resistivity, taken from Ref. 34 for samples $Fe_{1.086}Te$. Gray regions indicate the existence of structural transitions.

low-temperature modification is associated with a pronounced increase in the ratio c/a' (see below). Comparison of the diffraction patterns measured at temperatures above and below this phase transition reveals a close similarity of the diffraction intensities. Specifically, no evidence for extra reflections which would indicate, e.g., a doubling of a translation period is observed. Moreover, the diffraction diagrams of the low-temperature phase can still be indexed assuming tetragonal symmetry, and the same systematic absences of reflections are observed for the high- and the low-temperature phase. The corresponding diffraction symbol is compatible only with the centrosymmetric space groups $P4/n$ and $P4/nmm$. Inspection of the occupied Wyckoff positions ($2a$ and $2c$ in both space groups) immediately reveals that the coordinate triplets are the same for both choices. Thus, the higher Laue class was selected for the subsequent refinements. The least-squares-fit results of the structure models to the diffraction profiles measured above and below the transition at P3 and P4 are shown in Figs. 8(a)–8(d); the refined parameter values are summarized in Table III.

For a comparison of the metrical changes, the temperature dependence of the lattice parameters obtained from the refinements at ambient as well as at elevated pressures are summarized in Figs. 9(a)–9(j) and in Tables IV–VII (see Appendix). It can be seen that the symmetry-breaking transitions (tetragonal to monoclinic or to orthorhombic) are associated with a significantly anisotropic change of the unit cell dimensions [see Figs. 9(a)–9(f)]. In the case of the symmetry-conserving transition (tetragonal to tetragonal) the lattice parameter a contracts by $\approx$1% while c increases by approximately the same amount upon transforming into the low-temperature phase [see Figs. 9(g)–9(j)].

Putting some emphasis on the similarity between pressure and Fe excess, the temperature-induced changes of c/a' are compared for both parameters. Analysis of the ratio c/a' (in which $a' = a$ for tetragonal symmetry and $a' = \frac{1}{2}(a+b)$ for orthorhombic and monoclinic symmetries) reveals that the symmetry-breaking transitions at P0–P2 or compositions $Fe_{1+y}Te$ with $y = 0.06$–0.15 cause only minute changes of the ratio c/a', whereas the symmetry-conserving transition gives rise to a significantly more pronounced alteration [Figs. 10(a) and 10(b)].

IV. SUMMARY AND CONCLUSIONS

The anomaly that has been detected[34] in resistivity measurements on $Fe_{1.086}Te$ for pressures $p \leqslant 1$ GPa is conjectured to originate from a tetragonal-monoclinic phase transition. Our structure investigations confirm this picture. This phase transition occurs at $T_s \approx 65$ K. At somewhat higher pressures P2 ($\sim$1.4 GPa) [Fig. 9(e)], we clearly resolve a phase transition into the orthorhombic phase at $T \lesssim 60$ K. Yet, the change in c/a' at around 75 K is of similar magnitude as the alterations associated to the symmetry-breaking transitions at P0 and P1 around 60 K [see inset of Fig. 10(a)]. This pressure-driven subtle discontinuity within the tetragonal phase is consistent with a change observed for the onset of magnetic order in the temperature-composition phase diagram (Fig. 11). At still higher pressures, P3 and P4, we identify another

symmetry-conserving phase transition. The temperature of this transition increases with pressure, from ∼60 K at 2.29 GPa to ∼90 K at 2.9 GPa. There is no indication of the presence of any orthorhombic or monoclinic phases at these higher pressures. With this, one might speculate that the unidentified transition into phase HPII of Ref. 34 coincides with our symmetry-conserving phase transition.

Our pressure studies on $Fe_{1.08}Te$ here, along with our earlier investigations[29] on $Fe_{1+y}Te$ samples with different Fe excess $0.06 \leqslant y \leqslant 0.15$, suggest some analogy between the influence of pressure and Fe excess. These results together with results of Ref. 34 are summarized in Fig. 11 for comparison. For small pressures as well as for small Fe excess $y \leqslant 0.11$ we find a single transition from a tetragonal into a monoclinic low-temperature phase at roughly 60 K.[39] At a higher pressure $p \sim 1.5$ GPa or higher Fe excess $y \geqslant 0.13$ two successive transitions appear to take place. Consistently, the transition at lower temperature (∼46 K) results in an orthorhombic low-temperature phase. The second transition at somewhat higher temperature (e.g., at 57 K for $y = 0.13$) seems to retain the tetragonal symmetry but drives the material from a paramagnetic into a magnetically ordered phase. For even higher pressures $p \gtrsim 2.3$ GPa we find a symmetry-conserving phase transition. So far, no analogy to this latter transition has been observed for samples with increased Fe excess, likely because of the high amount of excess Fe beyond the homogeneity range of 6–15% that would be required. The exact nature of the magnetism in the tetragonal high-pressure phase remains to be investigated.

The close similarity of the temperature-composition and the temperature-pressure phase diagrams suggests a strong magnetoelastic coupling between the magnetic and structural order parameters in $Fe_{1+y}Te$. Paul *et al.*[40] presented a mean-field theory, in which symmetry-allowed magnetoelastic couplings give rise to monoclinic lattice distortion in the magnetic phase. The magnetoelastic couplings seem to vary with y. For $y \geqslant 0.12$, the magnetic structure becomes incommensurate with respect to the crystal lattice. Neutron-scattering studies report a helical modulation of the magnetic moments with a temperature-dependent propagation vector.[25,28] The structural transition into the orthorhombic phase at lower temperature takes place only when the magnetic propagation vector becomes temperature independent, i.e., at the lock-in transition.[29] Application of pressure induces increased overlap of the atomic orbitals which in turn tunes the magnetoelastic couplings. This results in similar magnetic structures as observed in $Fe_{1+y}Te$ with $y \geqslant 0.12$. The microscopic origin of the magnetic and crystal structures in this regime is not yet theoretically addressed.

In conclusion, we showed that pressure strongly influences the phase transitions of $Fe_{1.08}Te$ found at low temperatures. The temperature-dependent phase transitions can be successively changed from low-pressure tetragonal-monoclinic to tetragonal-orthorhombic followed by tetragonal-tetragonal with increasing compression. The pressure-dependent phase transitions closely resemble those induced by excess Fe composition.

Note added in proof. After submission of this article we recognize a report of an evolution of a two step structural phase transition, tetragonal-orthorhombic-monoclinic, with a two phase (monoclinic + orthorhombic) coexistence at low temperatures in $Fe_{1.13}Te$.[41]

ACKNOWLEDGMENTS

The authors wish to thank Yu. Grin, K. Koepernik, U. K. Rößler, and L. H. Tjeng for stimulating discussions. H. R. thanks Grant No. SPP 1458 and C.B. thanks the CNV foundation for financial support. We also acknowledge the ESRF for granting beam time at ID09A and ID31. Experimental support of Adrian Hill is highly appreciated.

APPENDIX: LATTICE PARAMETERS AT DIFFERENT TEMPERATURES AND PRESSURES

The various phase transitions as outlined in the main text are supported by the results of lattice parameter determinations at different pressures which are summarized in the following Tables IV–VII.

TABLE IV. Series P1: Experimental conditions (temperature, pressure) and lattice parameters determined by refinement of peak positions using full experimental diffraction profiles (LeBail fit). Average differences of temperature and pressure before and after the diffraction experiments amount to 0.1(1) K and 0.02(1) GPa, respectively.

Temperature (K)	Pressure (GPa)	a (Å)	b (Å)	c (Å)	β(deg)
296	0.31	3.808 76(3)	–	6.250 02(8)	–
200	0.74	3.790 60(2)	–	6.214 35(7)	–
150	0.73	3.784 97(2)	–	6.204 02(7)	–
100	0.71	3.785 60(1)	–	6.202 61(7)	–
80	0.63	3.787 85(2)	–	6.206 79(7)	–
70	0.59	3.788 86(2)	–	6.206 54(7)	–
65	0.58	3.790 04(3)	–	6.2076(1)	–
60	0.55	3.789 79(2)	–	6.2078(2)	–
55	0.53	3.798 45(7)	3.781 74(7)	6.2125(2)	90.191(3)
50	0.49	3.806 12(6)	3.776 99(5)	6.2180(2)	90.333(2)
45	0.53	3.809 75(7)	3.775 19(6)	6.2187(2)	90.399(2)

TABLE V. Series P2: Experimental conditions (temperature, pressure) and lattice parameters determined by refinement of peak positions using full experimental diffraction profiles (LeBail fit). Average differences of temperature and pressure before and after the diffraction experiments amount to 0.1(1) K and 0.02(1) GPa, respectively.

Temperature (K)	Pressure (GPa)	a (Å)	b (Å)	c (Å)
100	1.62	3.756 64(1)	–	6.1680(1)
80	1.63	3.756 66(1)	–	6.172 39(9)
75	1.49	3.762 08(2)	–	6.173 38(8)
70	1.47	3.761 78(1)	–	6.175 52(8)
65	1.44	3.761 72(2)	–	6.176 18(8)
60	1.42	3.762 00(2)	–	6.175 41(9)
55	1.40	3.769 65(6)	3.753 16(7)	6.1785(2)
50	1.36	3.770 82(6)	3.752 16(6)	6.1793(2)
45	1.41	3.773 32(5)	3.752 48(5)	6.1805(2)
40	1.40	3.774 87(5)	3.751 97(5)	6.1801(2)
35	1.40	3.776 14(5)	3.750 69(5)	6.1820(2)
30	1.37	3.777 40(6)	3.750 90(6)	6.1817(2)
27.5	1.38	3.777 88(6)	3.750 16(6)	6.1814(2)

TABLE VI. Series P3: Experimental conditions (temperature, pressure) and lattice parameters determined by refinement of peak positions using full experimental diffraction profiles (LeBail fit). Average differences of temperature and pressure before and after the diffraction experiments amount to 0.1(1) K and 0.02(1) GPa, respectively.

Temperature (K)	Pressure (GPa)	a (Å)	c (Å)
100[a]	2.47	3.727 42(2)	6.1377(2)
80[a]	2.44	3.726 44(2)	6.142 46(9)
60[b]	2.36	3.719 76(2)	6.1563(2)
40[a]	2.29	3.7284(5)	6.143(2)
40[c]	2.29	3.69615(2)	6.1996(1)
20[c]	2.33	3.69469(2)	6.2033(2)

[a]High-temperature phase.
[b]Average value for a mixture of the HT and LT phase since decomposition into the contributions of the components failed.
[c]Low-temperature phase.

TABLE VII. Series P4: Experimental conditions (temperature, pressure) and lattice parameters determined by refinement of peak positions using full experimental diffraction profiles (LeBail fit). Average differences of temperature and pressure before and after the diffraction experiments amount to 0.1(1) K and 0.02(1) GPa, respectively.

Temperature (K)	Pressure (GPa)	a (Å)	c (Å)
100[a]	2.86	3.713 43(1)	6.1323(2)
95[a]	2.89	3.710 17(1)	6.1341(2)
90[b]	2.91	3.704 64(1)	6.1421(2)
85[a]	2.92	3.7085(1)	6.125(5)
85[c]	2.92	3.690 71(6)	6.170(4)
80[a]	2.91	3.7065(2)	6.130(6)
80[c]	2.91	3.687 57(3)	6.171 (2)
75[c]	2.92	3.687 28(1)	6.1719(3)
70[c]	2.92	3.685 41(1)	6.1773(3)
65[c]	2.89	3.684 96(1)	6.1753(2)
60[c]	2.89	3.684 19(1)	6.1773(2)
55[c]	2.88	3.684 09(1)	6.1764(2)
50[c]	2.87	3.683 71(1)	6.1802(2)
45[c]	2.9	3.683 58(1)	6.1798(2)
40[c]	2.9	3.683 47(1)	6.1794(2)

[a]High-temperature phase.
[b]Average value for a mixture of the HT and LT phase since decomposition into the contributions of the components failed.
[c]Low-temperature phase.

*schwarz@cpfs.mpg.de

[1] Y. Kamihara, T. Watanabe, M. Hirano, and H. Hosono, J. Am. Chem. Soc. **130**, 3296 (2008).

[2] For a review of high-pressure studies, see C. W. Chu and B. Lorenz, Physica C **469**, 385 (2009).

[3] B. Lorenz, K. Sasmal, R. P. Chaudhury, X. H. Chen, R. H. Liu, T. Wu, and C. W. Chu, Phys. Rev. B **78**, 012505 (2008).

[4] M. Kumar, M. Nicklas, A. Jesche, N. Caroca-Canales, M. Schmitt, M. Hanfland, D. Kasinathan, U. Schwarz, H. Rosner, and C. Geibel, Phys. Rev. B **78**, 184516 (2008).

[5] H. Takahashi, K. Igawa, K. Arii, Y. Kamihara, M. Hirano, and H. Hosono, Nature (London) **453**, 376 (2008).

[6] S. K. Mishra, R. Mittal, S. L. Chaplot, S. V. Ovsyannikov, D. M. Trots, L. Dubrovinsky, Y. Su, Th. Brueckel, S. Matsuishi, H. Hosono, and G. Garbarino, Phys. Rev. B **84**, 224513 (2011).

[7] R. Mittal, S. K. Mishra, S. L. Chaplot, S. V. Ovsyannikov, E. Greenberg, D. M. Trots, L. Dubrovinsky, Y. Su, Th. Brueckel, S. Matsuishi, H. Hosono, and G. Garbarino, Phys. Rev. B **83**, 054503 (2011).

[8] H. Takahashi, H. Okada, K. Igawa, K. Arii, Y. Kamihara, S. Matsuishi, M. Hirano, H. Hosono, K. Matsubayashi, and Y. Uwatoko, J. Phys. Soc. Jpn. **77**, Suppl. C 78 (2008).

[9] H. Kotegawa, H. Sugawara, and H. Tou, J. Phys. Soc. Jpn. **78**, 013709 (2009).

[10] K. Igawa, H. Okada, H. Takahashi, S. Matsuishi, Y. Kamihara, M. Hirano, H. Hosono, K. Matsubayashi, and Y. Uwatoko, J. Phys. Soc. Jpn. **78**, 025001 (2009).

[11] E. Colombier, S. L. Bud'ko, N. Ni, and P. C. Canfield, Phys. Rev. B **79**, 224518 (2009).

[12] M. S. Torikachvili, S. L. Bud'ko, N. Ni, and P. C. Canfield, Phys. Rev. Lett. **101**, 057006 (2008).

[13] W. Yu, A. A. Aczel, T. J. Williams, S. L. Bud'ko, N. Ni, P. C. Canfield, and G. M. Luke, Phys. Rev. B **79**, 020511(R) (2009).

[14] A. Kreyssig, M. A. Green, Y. Lee, G. D. Samolyuk, P. Zajdel, J. W. Lynn, S. L. Bud'ko, M. S. Torikachvili, N. Ni, S. Nandi, J. B. Leão, S. J. Poulton, D. N. Argyriou, B. N. Harmon, R. J. McQueeney, P. C. Canfield, and A. I. Goldman, Phys. Rev. B **78**, 184517 (2008).

[15] W. Uhoya, A. Stemshorn, G. Tsoi, Y. K. Vohra, A. S. Sefat, B. C. Sales, K. M. Hope, and S. T. Weir, Phys. Rev. B **82**, 144118 (2010).

[16] D. Kasinathan, M. Schmitt, K. Koepernik, A. Ormeci, K. Meier, U. Schwarz, M. Hanfland, C. Geibel, Y. Grin, A. Leithe-Jasper, and H. Rosner, Phys. Rev. B **84**, 054509 (2011).

[17] F.-C. Hsu, J.-Y. Luo, K.-W. Yeh, T.-K. Chen, T.-W. Huang, P. M. Wu, Y.-C. Lee, Y.-L. Huang, Y.-Y. Chu, D.-C. Yan, and M.-K. Wu, Proc. Natl. Acad. Sci. USA **105**, 14262 (2008).

[18] T. M. McQueen, A. J. Williams, P. W. Stephens, J. Tao, Y. Zhu, V. Ksenofontov, F. Casper, C. Felser, and R. J. Cava, Phys. Rev. Lett. **103**, 057002 (2009).

[19] Y. Mizuguchi, F. Tomioka, S. Tsuda, T. Yamaguchi, and Y. Takano, Appl. Phys. Lett. **93**, 152505 (2008).

[20] S. Medvedev, T. M. McQueen, I. A. Troyan, T. Palasyuk, M. I. Eremets, R. J. Cava, S. Naghavi, F. Casper, V. Ksenofontov, G. Wortmann, and C. Felser, Nat. Mater. **8**, 630 (2009).

[21] S. Margadonna, Y. Takabayashi, Y. Ohishi, Y. Mizuguchi, Y. Takano, T. Kagayama, T. Nakagawa, M. Takata, and K. Prassides, Phys. Rev. B **80**, 064506 (2009).

[22] K.-W. Yeh, T.-W. Huang, Y.-L. Huang, T.-K. Chen, F.-C. Hsu, P. M. Wu, Y.-C. Lee, Y.-Y. Chu, C.-L. Chen, J.-Y. Luo, D.-C. Yan, and M.-K. Wu, Europhys. Lett. **84**, 37002 (2008).

[23] M. H. Fang, H. M. Pham, B. Qian, T. J. Liu, E. K. Vehstedt, Y. Liu, L. Spinu, and Z. Q. Mao, Phys. Rev. B **78**, 224503 (2008).

[24] S. Rößler, D. Cherian, S. Harikrishnan, H. L. Bhat, S. Elizabeth, J. A. Mydosh, L. H. Tjeng, F. Steglich, and S. Wirth, Phys. Rev. B **82**, 144523 (2010).

[25] W. Bao, Y. Qiu, Q. Huang, M. A. Green, P. Zajdel, M. R. Fitzsimmons, M. Zhernenkov, S. Chang, M. Fang, B. Qian, E. K. Vehstedt, J. Yang, H. M. Pham, L. Spinu, and Z. Q. Mao, Phys. Rev. Lett. **102**, 247001 (2009).

[26] S. Li, C. de la Cruz, Q. Huang, Y. Chen, J. W. Lynn, J. Hu, Y.-L. Huang, F.-C. Hsu, K.-W. Yeh, M.-K. Wu, and P. Dai, Phys. Rev. B **79**, 054503 (2009).

[27] R. Hu, E. S. Bozin, J. B. Warren, and C. Petrovic, Phys. Rev. B **80**, 214514 (2009).

[28] E. E. Rodriguez, C. Stock, P. Zajdel, K. L. Krycka, C. F. Majkrzak, P. Zavalij, and M. A. Green, Phys. Rev. B **84**, 064403 (2011).

[29] S. Rößler, D. Cherian, W. Lorenz, M. Doerr, C. Koz, C. Curfs, Yu. Prots, U. K. Rößler, U. Schwarz, S. Elizabeth, and S. Wirth, Phys. Rev. B **84**, 174506 (2011).

[30] I. A. Zaliznyak, Z. J. Xu, J. S. Wen, J. M. Tranquada, G. D. Gu, V. Solovyov, V. N. Glazkov, A. I. Zheludev, V. O. Garlea, and M. B. Stone, Phys. Rev. B **85**, 085105 (2012).

[31] C. Zhang, W. Yi, L. Sun, X.-J. Chen, R. J. Hemley, H.-K. Mao, W. Lu, X. Dong, L. Bai, J. Liu, A. F. Moreira Dos Santos, J. J. Molaison, C. A. Tulk, G. Chen, N. Wang, and Z. Zhao, Phys. Rev. B **80**, 144519 (2009).

[32] J.-E. Jørgensen, J. S. Olsen, and L. Gerward, High Pressure Res. **31**, 603 (2011).

[33] Note that some authors use $FeTe_{1-\delta}$ rather than $Fe_{1+y}Te$. Since experimental evidence for substantial chalcogen vacancies is lacking, the latter notation is more frequently used. Here, $FeTe_{0.92}$ corresponds to $Fe_{1.086}Te$.

[34] H. Okada, H. Takahashi, Y. Mizuguchi, Y. Takano, and H. Takahashi, J. Phys. Soc. Jpn. **78**, 083709 (2009).

[35] WinCSD, L. G. Akselrud, P. Y. Zavalii, Yu. Grin, V. K. Pecharsky, B. Baumgartner, and E. Wölfel, Mater. Sci. Forum **133–136**, 335 (1993).

[36] JANA: V. Petricek, M. Dusek, and L. Palatinus, JANA 2006. The Crystallographic Computing System, Institute of Physics, Praha, Czech Republic, www-xray.fzu.cz/jana.

[37] A. March, Z. Kristallogr. **81**, 285 (1932).

[38] W. A. Dollase, J. Appl. Crystallogr. **19**, 267 (1986).

[39] There are minor differences in the transition temperatures as determined by structural investigations at ambient pressure in this work and for the sample with $y = 0.08$ by thermodynamic and magnetic measurements.[29] These small differences are assigned to the different cooling protocols and a possible difference in the estimated chemical composition.

[40] I. Paul, A. Cano, and K. Sengupta, Phys. Rev. B **83**, 115109 (2011).

[41] Y. Mizuguchi, K. Hamada, K. Goto, H. Takatsu, H. Kadowaki, and O. Miura, Solid State Commun. **152**, 1047 (2012).